

NO-A100 790

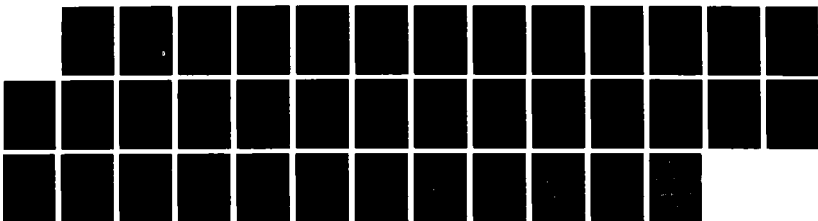
THERMAL OXIDE GROWTH ON SILICON: INTRINSIC STRESS AND  
SILICON CLEANING EFFECTS(U) NORTH CAROLINA UNIV AT  
CHAPEL HILL DEPT OF CHEMISTRY E A IRENE 03 DEC 87  
TR-19 N00014-86-K-0305

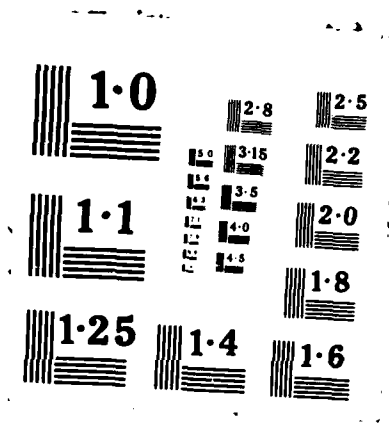
1/1

UNCLASSIFIED

F/G 7/2

NL





1.0

2.8

2.5

1.1

3.0

3.15

2.2

3.5

4.0

4.5

2.0

1.25

1.4

1.8

1.6

AD-A188 790

OFFICE OF NAVAL RESEARCH  
CONTRACT NO. N00014-86-K-0305  
TECHNICAL REPORT NO. 19

Thermal Oxide Growth on Silicon: Intrinsic Stress & Silicon  
Cleaning Effects

E.A. Irene  
Department of Chemistry  
University of North Carolina  
Chapel Hill, NC 27514

in  
Symposium Volume of American Vacuum Society

DTIC  
SELECTED  
DEC 28 1987  
S E D

Reproduction in whole or in part is permitted for any purpose of the United States Government.

This document has been approved for public release and sale; its distribution is unlimited.

87 12 14 058

A128 790

## REPORT DOCUMENTATION PAGE

1a. REPORT SECURITY CLASSIFICATION Unclassified		1b. RESTRICTIVE MARKINGS	
2a. SECURITY CLASSIFICATION AUTHORITY		3. DISTRIBUTION/AVAILABILITY OF REPORT Approved for public release; distribution unlimited.	
2b. DECLASSIFICATION/DOWNGRADING SCHEDULE			
4. PERFORMING ORGANIZATION REPORT NUMBER(S) Technical Report #19		5. MONITORING ORGANIZATION REPORT NUMBER(S)	
6a. NAME OF PERFORMING ORGANIZATION UNC Chemistry Dept.	6b. OFFICE SYMBOL (If applicable)	7a. NAME OF MONITORING ORGANIZATION Office of Naval Research (Code 413)	
6c. ADDRESS (City, State and ZIP Code) 11-3 Venable Hall 045A Chapel Hill, NC 27514		7b. ADDRESS (City, State and ZIP Code) Chemistry Program 800 N. Quincy Street Arlington, Virginia 22217	
8a. NAME OF FUNDING/SPONSORING ORGANIZATION Office of Naval Research	8b. OFFICE SYMBOL (If applicable)	9. PROCUREMENT INSTRUMENT IDENTIFICATION NUMBER Contract #N00014-86-K-0305	
8c. ADDRESS (City, State and ZIP Code) Chemistry Program 800 N. Quincy Street, Arlington, VA 22217		10. SOURCE OF FUNDING NOS	
		PROGRAM ELEMENT NO.	PROJECT NO.
		TASK NO.	WORK UNIT NO.
11. TITLE (Include Security Classification) THERMAL OXIDE GROWTH ON SILICON: INTRINSIC STRESS & SILICON			
12. PERSONAL AUTHOR(S) CLEANING EFFECTS			
E.A. Irene			
13a. TYPE OF REPORT Interim Technical	13b. TIME COVERED FROM _____ TO _____	14. DATE OF REPORT (Yr., Mo., Day) December 3, 1987	15. PAGE COUNT 36
18. SUPPLEMENTARY NOTATION Symposium Volume of American Vacuum Society			
17. COSATI CODES		18. SUBJECT TERMS (Continue on reverse if necessary and identify by block number)	
FIELD	GROUP	SUB. GR.	
			SILICON, silicon oxide
19. ABSTRACT (Continue on reverse if necessary and identify by block number)			
<p>This paper summarizes the experimental results and discusses the implications of recent research on two topics related to Si oxidation: mechanical stress effects; and the influence of impurities on the Si surface. For stress measurement, a double beam optical technique is used to measure the strain in the Si substrate due to the film stress. An intrinsic <math>\text{SiO}_2</math> stress is measured which increases with decreasing oxidation temperature. Controversy exists about whether the intrinsic stress affects transport of oxidant or the interface reaction; arguments for both views are presented. A combination of in-situ ellipsometry and contact angle measurements performed on a Si surface which is immersed in various liquid media has been successfully used to determine the role of HF in Si cleaning process. A fluorocarbon film was found to replace the removed <math>\text{SiO}_2</math>, and the fluorocarbon renders the Si surface hydrophobic and amenable to the growth of a high quality <math>\text{SiO}_2</math> film for device applications.</p>			
20. DISTRIBUTION/AVAILABILITY OF ABSTRACT UNCLASSIFIED/UNLIMITED <input checked="" type="checkbox"/> SAME AS RPT <input type="checkbox"/> DTIC USERS <input type="checkbox"/>		21. ABSTRACT SECURITY CLASSIFICATION Unclassified	
22a. NAME OF RESPONSIBLE INDIVIDUAL Dr. David L. Nelson		22b. TELEPHONE NUMBER (Include Area Code) (202) 696-4410	22c. OFFICE SYMBOL

Thermal Oxide Growth on Silicon: Intrinsic Stress and Silicon  
Cleaning Effects

E. A. Irene  
Department of Chemistry  
University of North Carolina  
Chapel Hill, North Carolina 27514

Abstract

This paper summarizes the experimental results and discusses the implications of recent research on two topics related to Si oxidation: mechanical stress effects; and the influence of impurities on the Si surface. For stress measurement, a double beam optical technique is used to measure the strain in the Si substrate due to the film stress. An intrinsic SiO<sub>2</sub> stress is measured which increases with decreasing oxidation temperature. Controversy exists about whether the intrinsic stress affects transport of oxidant or the interface reaction; arguments for both views are presented. A combination of in-situ ellipsometry and contact angle measurements performed on a Si surface which is immersed in various liquid media has been successfully used to determine the role of HF in Si cleaning process. A fluorocarbon film was found to replace the removed SiO<sub>2</sub>, and the fluorocarbon renders the Si surface hydrophobic and amenable to the growth of a high quality SiO<sub>2</sub> film for device applications.



Accession For	
NTIS GRA&I	<input checked="" type="checkbox"/>
DTIC TAB	<input type="checkbox"/>
Unannounced	<input type="checkbox"/>
Justification	
By _____	
Distribution/	
Availability Codes	
Dist	Avail and/or Special
A-1	

## Introduction

The clear trend in silicon Microelectronics processing is towards lower process temperatures (1,2). The motivation is to reduce the diffusion of dopants and thereby to protect diffused junctions and eliminate unwanted interface reactions. This issue arises directly from the industrial effort to reduce device size and thereby increase the level of integration. The impact on the Si thermal oxidation process is profound and several real scientific issues emerge. Firstly, the reduction in lateral size of individual devices on a chip also requires a reduction in the gate area,  $A$ , of MOS devices. As seen in equation (1), in order to maintain the same device operating characteristics, viz., the device capacitance,  $C$ , because of the reduction of  $A$ , the oxide film thickness,  $L_o$ , must also be reduced since

$$C = KA/L_o \quad (1)$$

where  $K$  is the dielectric constant for the  $SiO_2$  film. The scientific issue here is that the contemplated integration schemes have driven the thickness range for  $SiO_2$  films to below 20 nm. However, based on many recent studies, the presently accepted oxidation model, the Linear-Parabolic, L-P, model (3-5), is considered to be inapplicable for dry oxidations below about 30 nm  $SiO_2$  thickness. In fact the L-P model is usually derived to contain an offset,  $L_o$ , to avert the thin film regime below several tens of nm as:

$$t-t_0 = (L-L_0)/k_1 + (L^2-L_0^2)/k_2 \quad (2)$$

where  $L$  and  $t$  are the  $\text{SiO}_2$  thickness and time,  $L_0$  and  $t_0$  represent the small thickness region in  $L$ ,  $t$  space which does not fit the model, viz. the offset region,  $k_1$  and  $k_2$  are the linear and parabolic rate constants, respectively (5). The initial regime, for  $L < L_0$ , is characterized by faster than usual oxidation kinetics. Further scientific investigation is required to determine the reasons why this regime is different from the L-P regime. Impurities are known to have a profound effect on this regime (6-8), and we will summarize some recent research in this area that is aimed at an understanding of impurity effects on the Si surface. Secondly, the required reduction in process temperatures directly affects some  $\text{SiO}_2$  film properties (9). In particular, intrinsic film stress,  $\sigma_i$ , film density,  $\rho$ , Si-SiO<sub>2</sub> interfacial fixed charge,  $Q_f$ , and possibly Si-SiO<sub>2</sub> interface states,  $Q_{it}$ , all increase with decreasing oxidation temperature and all anneal to lower temperatures as depicted in Figure 1. These properties may also affect the Si oxidation mechanism. In this paper, some current research on impurity effects and mechanical stress effects on the Si oxidation mechanism is discussed. A recent review (ref. 10 and references therein) presents a more complete picture of the silicon oxidation problem. We commence with a summary of stress effects.

#### Stress Effects on Si Oxidation

### Stress Relationships

Two components of the residual film stress,  $\sigma$ , are discussed: thermal stress,  $\sigma_{t,n}$ , and intrinsic stress,  $\sigma_i$ , and these are additive as:

$$\sigma = \sigma_{t,n} + \sigma_i \quad (3)$$

The thermal stress or thermal expansion stress is attributed to the difference in thermal expansion coefficients,  $\Delta\alpha$ , between the  $\text{SiO}_2$  film and the Si substrate as:

$$\Delta\alpha = \alpha(\text{SiO}_2) - \alpha(\text{Si}) \quad (4)$$

which when multiplied by the difference between the film growth temperature,  $T_o$ , and stress measurement temperature  $T$ ,  $\Delta T = (T_o - T)$  and then multiplied by Youngs modulus,  $E$ , divided by  $(1 - \nu)$  where  $\nu$  is Poissons ratio for the film yields an expression for the thermal stress:

$$\sigma_{t,n} = \Delta\alpha \cdot \Delta T \cdot [E / (1 - \nu)] \quad (5)$$

It should be clearly understood that  $\sigma_{t,n}$  cannot affect the oxidation reaction itself, since from eqn. (5)  $\Delta T = 0$  at  $T = T_o$  and thus  $\sigma_{t,n} = 0$  at the oxidation temperature. For  $\text{SiO}_2$  on Si,  $\alpha(\text{SiO}_2) < \alpha(\text{Si})$ , hence  $\Delta\alpha$  is negative and a compressive thermal stress results upon cooling from  $T_o$  to room temperature, i.e.,

$\sigma_{t,n}$  is negative. The higher  $T_{ox}$ , the larger would be  $\sigma_{t,n}$  as measured at room temperature. Measurements done with oxides grown at high oxidation temperatures of 1000°C and above (11,12) have yielded stress results which are totally consistent with  $\sigma = \sigma_{t,n}$  ( $\sigma_i = 0$ ), viz. with a numerical value from the above expression for  $\sigma_{t,n}$  and a larger room temperature value for larger  $T_{ox}$  values. However, for oxides grown at lower oxidation temperatures, evidence for a non-zero intrinsic component was reported (13,14). In-situ stress measurements at  $T_{ox}$  (where  $\sigma_{t,n} = 0$ ) have shown that  $\sigma_i$  is also compressive and increases with decreasing  $T_{ox}$  (i.e. oppositely to the temperature dependence of  $\sigma_{t,n}$ ). The origin for this intrinsic stress was proposed to be due to the large molar volume change,  $\Delta V$ , for the conversion of Si to  $SiO_2$  which is 120% or a factor of 2.2x (14-16). The direction and order of magnitude of this stress has been confirmed (17,18).

#### Film Stress Techniques

Before proceeding to a summary of the stress measurements results, it would be useful to present a brief description of several stress measurement methods recently applied to  $SiO_2$  films. Virtually all of the experimental measurements determine the strain or the deformation in the substrate, as caused by a thin uniform film on one surface of the substrate. The strain is directly proportional to stress in the elastic limit, and for the case of the substrate thickness being much larger than the film thickness, the film stress,  $\sigma_f$ , can be related to the radius of curvature,  $R$ , of the substrate through Stoney's formula (19):

$$\sigma_f = [E \cdot L_s \cdot \epsilon / (6 \cdot (1 - \nu) \cdot L_f)] / R \quad (5)$$

where the elastic constants are for the substrate which is deforming and  $L_s$  and  $L_f$  are the thicknesses for the substrate and film respectively. Thus the experimental techniques are aimed at measuring  $R$ . Three general classes of measurements are routinely found in the literature: mechanical, diffraction, and optical. These differ in the manner in which  $R$  is measured and under each general class usually several techniques have been developed. A more complete discussion of film stress measurement will be reserved for a separate review, and herein we discuss only specific reports of stress in  $\text{SiO}_2$  films on Si substrates. The most recent reports have employed x-ray diffraction and optical techniques (13, 14, 17, 18).

One prominent x-ray technique is based on the maintenance of the Bragg condition for diffraction from thin Si substrates (21, 22). Essentially, the single crystal Si substrate is brought under Bragg conditions with respect to the incident x-ray beam, through the use of major reflections for the specific Si orientation used. While monitoring the diffracted radiation at the Bragg angle,  $\theta$ , the sample is traversed relative to the beam while keeping the same angle to the beam. If the sample is perfectly flat, the crystal planes remain with constant angles to the x-ray beam and the Bragg conditions are maintained. If, however, the Si substrate is curved as a result of film stress,

then upon traversing the sample in front of the beam, the Bragg condition will be lost and an adjustment in the crystal position will be required to reattain the Bragg condition. The amount of adjustment depends both on the substrate radius of curvature,  $R$ , which is to be measured and the distance the sample is traversed which is known. This measurement apparatus is often automated and called ABAC for automated Bragg angle camera. The advantages of this technique is the great sensitivity to stresses as low as  $10^7$  dyne/cm<sup>2</sup> and absolute reference from the lattice planes in the single crystal substrate. The disadvantage is expense and complexity, as a high intensity x-ray source, diffraction camera, and associated automation apparatus are required.

A number of optical techniques have been used on SiO<sub>2</sub> films. One is the so-called Newton rings technique which makes use of the optical interference pattern caused by combining the reflections from the surface of an optical flat and a curved surface in contact with the flat (23,24). Using monochromatic light, a series of rings result, Newtons rings, the number of which in a certain distance, the separation, is proportional to the curvature of the surface,  $R$ . If very uniform surfaces are obtained, this technique can be useful for stresses of about  $10^9$  dynes/cm<sup>2</sup> and upwards. Cleanliness of the surfaces in contact is a problem as is obtaining flat or uniformly curved substrates for the measurements.

Two other optical reflection techniques have been reported. One technique uses the reflection of one narrow light beam from a

film covered surface (see for example ref. (25)). The argument here is that the reflected beam will be undeviated from a flat surface which is traversed during reflection. If the surface is curved, a deviation of the reflected beam will occur. As in the ABAC case, the deviation can be geometrically related to  $R$ . However, it is easy to show that a deviation due to curvature of the substrate is difficult, if not impossible, to distinguish from misalignment of a flat sample. Both situations would cause reflected beam deviation. Thus, this technique is difficult to use without unambiguous alignment procedures which, to this authors knowledge, have not been reported. The difficulty with the single beam technique is obviated with the use of two parallel reflected beams. An experimental apparatus is shown in Figure 2 (17,18). The laser light is split (at BS1) then reflected onto a silvered prism and adjusted so that the reflected beams are parallel. The parallel beams are again split (at BS2) with half going to a screen and forming two reference spots of separation  $X$ . The other is reflected from the sample surface, across the lab, in order to obtain a lever effect, and then to another plane mirror (M3) and finally to the same screen. If the sample is perfectly flat, the two sets of spots have the same  $X$  separation; but if the sample is curved, then a different separation,  $S$ , for the second set of spots is seen, viz. the reflections from the sample.  $R$  is then easily calculated from the difference between  $R$  and  $X$  and the measurement geometry. This technique has the decided advantages of being able to

distinguish sample tilt from curvature, and to be absolutely calibrated. For sample tilt, the two beams would be deviated in a parallel fashion in one direction, but for curvature only the spot separation changes. To insure beam parallelism, a flat mirror is substituted for the sample and the apparatus is adjusted such that the two sets of spots are identical. For calibration of R, commercially available precision spherical mirrors with known R replace the sample thus calibrating the apparatus geometry. The results from this technique have been found to be quite reproducible and are emphasized in the discussion to follow.

#### SiO<sub>2</sub> Film Stress Results

The first studies of the SiO<sub>2</sub> film stress (11,12) were performed using SiO<sub>2</sub> films grown at temperatures of 1000°C and higher which were appropriate processing temperatures for that era. These studies used predominantly mechanical measurements of R and were concordant in that they reported residual room temperature stress values that could be completely explained based on the anticipated value for the thermal expansion stress from equation (5) above. Hence, no evidence for an intrinsic SiO<sub>2</sub> stress was reported. From these studies, there was no reason to include stress in any oxidation models, because at oxidation temperature  $\sigma_{,n} = 0$ . More recent results using a double beam reflection technique in the Si oxidation environment, in-situ, revealed that a compressive intrinsic stress exists at temperatures less than 1000°C and this stress was found to

increase as the oxidation temperature decreased (13). This direction of change of the intrinsic stress with oxidation temperature is opposite to that anticipated for the temperature variation of the thermal stress as obtained from equation (5). Thus, this newly measured intrinsic stress is easily discerned even in the presence of the thermal expansion stress. Of course the in-situ measurement at the oxidation temperature insures that  $\sigma_{\text{th}} = 0$ , hence no confusion results. More recent room temperature stress measurements using the ABAC technique (14) and the double beam reflection technique (17,18), have confirmed that an intrinsic  $\text{SiO}_2$  film stress exists. Figure 3 shows a plot of total room temperature  $\text{SiO}_2$  film stress measurements along with the calculated thermal expansion film stress resulting from equation (5) all as a function of the thermal oxidation temperature. The differences in the temperature variation for these two stress components is evident. Figure 4 shows  $\sigma_i$ , which is the difference in the total and thermal stress against oxidation temperature.  $\sigma_i$  is seen to decrease with increasing oxidation temperature.

The origin and temperature dependence of  $\sigma_i$  is understood by considering the large molar volume change,  $\Delta V$ , for the conversion of Si to  $\text{SiO}_2$ , and the viscoelastic nature of  $\text{SiO}_2$  (14-16). From figure 5, we see that the as-formed  $\text{SiO}_2$  occupies a greater volume than the Si from which it was produced, hence an expansion needs to occur into the free volume direction above the oxidizing Si surface. Using a Maxwell model for  $\text{SiO}_2$ , the rate at which the flow of  $\text{SiO}_2$  can occur into this free direction is determined

by the  $\text{SiO}_2$  viscosity,  $\eta$ . At high oxidation temperatures where  $\eta$  is sufficiently small, the  $\text{SiO}_2$  flows readily into the free direction with a short relaxation time relative to the time for oxidation. At lower temperatures, (below about  $900^\circ\text{C}$ ), however,  $\eta$  is too large for complete relaxation, hence  $\sigma_i$  develops. The lower is  $T_o$ , the higher is  $\eta$ , and the higher is  $\sigma_i$ . Relaxation time calculations seem to confirm this viscoelastic model for  $\text{SiO}_2$  (14).

In terms of the relationship of  $\sigma_i$  to Si oxidation models, two different ideas have arisen. The first deals with the compressive  $\sigma_i$  in the  $\text{SiO}_2$  film. This compression ought to reduce the diffusivity of  $\text{O}_2$ , hence the supply of  $\text{O}_2$  to fuel the oxidation reaction. Thus a decrease in the oxidation rate should occur due to  $\sigma_i$ . Some confirmation for this exists from recent experiments (26) that show that when  $\sigma_i$  is released by long term annealing of thick  $\text{SiO}_2$  films, the oxidation rate increases. Considering the molar volume change as the origin of  $\sigma_i$ , the stress distribution in the  $\text{SiO}_2$  film should result in a large stress near the Si- $\text{SiO}_2$  interface with a decreasing stress towards the  $\text{SiO}_2$  surface. This would result in a higher  $\sigma_i$  and a reduced oxidation rate for thinner  $\text{SiO}_2$  films. However, it is well known that a higher oxidation rate is seen for thin films (less than  $200\text{\AA}$ ), yet the shape of the thin  $\text{SiO}_2$  oxidation data is explained by this model (27-29). Most recent  $\sigma_i$  measurements (20) have shown that indeed a higher stress exists for thinner films, but not as high as would be required from these diffusion

models.

The second stress related oxidation model is derived from the fact that the compressive  $\sigma_c$  in  $\text{SiO}_2$  gives rise to a tensile stress at the Si surface. The resulting strained Si bonds ought to yield a more reactive Si surface thereby enhancing the rate of oxidation(30). This idea seems in accord with the observation of faster oxidation rates for thinner films, where the Si- $\text{SiO}_2$  interface is kinetically most important, and some direct evidence for an enhanced rate of oxidation for tensile loaded Si has been presented (31). However, while there seems to be qualitative agreement with the model, quantitative scaling of the oxidation rate with  $\sigma_c$  is not found (32,33) and the predicted orientation dependence for the stress is not observed (18).

From Figure 6, it is seen that the intrinsic stresses for the (100), (110) and (311) Si orientations are near to each other and larger than the stress in the (111) surface. The order for oxidation rate (30,32,33) at the outset of oxidation is:

$$(110) > (111) > (311) > (100)$$

However, after several tens of nm  $\text{SiO}_2$  growth, the order changes to:

$$(111) > (110) > (311) > (100)$$

The initial oxidation regime scales qualitatively with the number density of Si atoms in the various Si orientations, but after this regime, the change in order may be a result of the reduced compressive stress in the  $\text{SiO}_2$ , since the scaling then appears to be in the order of smaller stress higher oxidation rate (33).

Since the initial oxidation rate does not scale quantitatively with the number density of Si atoms, and a crossover in rate order occurs for greater film thicknesses, a role for stress in the oxidation mechanism can be envisaged, but it should be clear that any definitive statements about the role of  $\sigma$ , on Si oxidation kinetics requires further investigation.

#### Impurity Effects on Si Oxidation

It has long been recognized (6,7) that a variety of impurities can alter the rate of Si oxidation, the mechanism for oxidation, and in many cases the resultant interfacial Si-SiO<sub>2</sub> electronic properties. One difficulty with the detailed investigation of these effects is that the chemical analyses used to identify and quantify many of the affecting impurities is far less sensitive to the impurity than is the electronic property or oxidation rate which is altered as a result of the presence of an impurity. However, while the oxidation rate and electronic effects are sensitive, they are not specific and thus there has been great difficulty in establishing clear cause and effect relationships. A similar situation surrounds our understanding of the details of the cleaning process of semiconductor surfaces. Virtually all common semiconductors are subjected to wet and/or dry chemical processes prior to commencing the device fabrication process (34-36). This exposure is usually termed "cleaning" and the intent is to remove any impurities. However, it is well known that for many of the cases examined, some impurities are

indeed removed but often impurities are merely replaced. The success of such a cleaning process relies on the innocuous nature of replacement impurities.

Some recent research in the area of impurities and impurity effects suggests that sensitive analytical techniques applied during the cleaning process, so called "in-situ" analysis should prove useful in elucidating the area of semiconductor surface cleaning and the role of impurities (7,8,37). Among the techniques explored and herein reported are in-situ ellipsometry and in-situ contact angle used in the solution cleaning environment of Si.

#### In-situ Solution Techniques

A. Ellipsometry. Ellipsometry is known to be sensitive to submonolayer coverage of a surface (38). The measurables in ellipsometry are the amplitude change in the light upon reflection,  $\Psi$ , and the phase change,  $\Delta$ . The measurables are related to the other parameters of the reflection problem as:

$$\tan\Psi\exp(i\Delta) = f(n_A, n_F, n_S, \lambda, \varphi) \quad (6)$$

where the n's are refractive indices (which are in general complex) for the ambient, A, film, F and substrate, S, respectively and  $\lambda$  is the wavelength,  $L_F$ , the film thickness and  $\varphi$  the angle of incidence. Usually  $n_A$ ,  $n_S$ ,  $\varphi$ , and  $\lambda$  are known. Thus from a single measurement of  $\Psi$  and  $\Delta$ ,  $n_F$  and  $L_F$  are obtained assuming that  $n_F$  is real. Figure 7 shows the fused silica sample cell used for the in situ measurements. Alignment of this cell with sample vertical in the solution was a non trivial procedure

with the details in the literature (37).

B. Contact Angle. The contact angle,  $\theta$ , is defined by the equilibrium of three surface tension vectors,  $\gamma_{i,j}$ , at the solid, S, liquid, L, vapor, V, interface as  $\gamma_{s,v}$ ,  $\gamma_{s,l}$ ,  $\gamma_{l,v}$ :

$$\cos\theta = (\gamma_{s,v} - \gamma_{s,l})/\gamma_{l,v} \quad (7)$$

Figure 8 shows the relationship. Usually only  $\gamma_{l,v}$  is known for a liquid, so that since  $\theta$  is measured only the difference  $\gamma_{s,v} - \gamma_{s,l}$  is obtained. Yet the wetting behavior of solids is directly related to  $\theta$  where large angles indicate hydrophobic behavior (non wetting) and small angles hydrophilic behavior (wetting). Most metals, oxides, and semiconductors are high energy solids with surface tensions,  $\gamma_{s,l}$ 's, of from 500 to 5000 dynes/cm. Waxes and some polymers are low energy solids with surface tensions of less than 100 dynes/cm. Virtually all liquids, except liquid metals, have surface tensions less than 100 dynes/cm. From these values, it can be argued on thermodynamic grounds that virtually all liquids will wet most solids, so as to lower the surface energy of the solid and thus yield a small, hydrophilic  $\theta$ . It has been shown that the critical surface tension,  $\gamma_c$ , obtained when  $\cos\theta = 1$  and thus  $\gamma_c = \gamma_{l,v} = (\gamma_{s,v} - \gamma_{s,l})$  is specifically related to the surface structure and composition of a solid surface (39).

For the measurement of  $\theta$  on semiconductor surfaces, during cleaning, and with the surface protected from the atmosphere, an inverted bubble technique (40) was adapted. The apparatus used for the experimental results and the experimental details are

reported elsewhere (37). A gas bubble ( $N_2$ ) can be released from the capillary and when held at the solid surface will establish the three phase equilibrium. It is important to realize that even though the bubble here is gas, the contact angle measured is the same as for the case shown in Figure 8 .

#### Results of In-situ Ellipsometric and Contact Angle Measurements

The first experimental result makes use of in-situ ellipsometry to follow the process of HF etching of  $SiO_2$  on Si. The use of HF in Si technology is widespread for both the patterning and complete removal of  $SiO_2$  from Si and the pre processing cleaning step to remove a contaminated or damaged native  $SiO_2$  film. Furthermore, it is established that the exposure of Si to HF alters the oxidation rate of Si(7,37). The use of HF is an integral part of the successful cleaning of Si. It is anticipated that the etching process of  $SiO_2$  in dilute HF should be able to be followed using in-situ ellipsometry, and Figure 9 shows the rather linear decrease in  $SiO_2$  film thickness with etch time. In this experiment, it was expected that the bare Si surface would be reached. This seems not to be the case, as a minimum of about 20Å  $SiO_2$  film thickness is reached, and it even appears as if the oxide grows slightly. However, in order to correctly interpret these results, it must be remembered that an ellipsometric model of the film covered surface is required for the analysis of the  $\Psi, \Delta$  data obtained during the etching process. Up to here, we have used model comprised of three components: air -  $SiO_2$  film - Si substrate and the  $\Psi, \Delta$  data is

always interpreted in terms of a calculated  $\text{SiO}_2$  film thickness. It is seen in Figure 9 that this model works quite well down to about 20Å but below this  $\text{SiO}_2$  thickness, the situation is not as clear. Using this simple model, the  $\text{SiO}_2$  etching first nearly ceases and then the  $\text{SiO}_2$  grows. Neither of these events is entirely plausible considering what we know about the virulence of the HF attack on  $\text{SiO}_2$ . If the  $\psi, \Delta$  trajectory is tracked below 20Å as the  $\text{SiO}_2$  film is removed, the situation becomes somewhat clarified and this unmodeled data is shown in Fig. 10. The solid line represents a theoretical calculation of  $\psi, \Delta$  values for the situation: air -  $\text{SiO}_2$  film - Si substrate. The zero  $\text{SiO}_2$  film thickness, i.e.  $\psi, \Delta$  for a bare Si surface is about  $178^\circ, 10.5^\circ$  and as  $\text{SiO}_2$  grows,  $\Delta$  decreases and  $\psi$  increases. The etch experiment shown in Fig. 10 commenced at an  $\text{SiO}_2$  film thickness of 85nm with a  $\psi, \Delta$  of about  $103^\circ, 15.5^\circ$  and proceeds towards the bare Si surface value with increasing  $\psi$  along the theoretical curve (open circles). Excellent agreement is seen along this line from 85 to about 2nm. However, near the 2nm  $\psi, \Delta$  value, a deviation from the theoretical curve is seen (triangles) with  $\Delta$  decreasing again and  $\psi$  increasing, but for  $\psi$  a much slower increase than if the correct model included a growing  $\text{SiO}_2$  film. Thus, while a value of 2-3nm for  $\text{SiO}_2$  is obtained for the  $\psi, \Delta$  data in the triangle region, the data is seen to deviate substantially from the theoretical curve for  $\text{SiO}_2$  on Si and hence from the simple model for a film on a substrate. This strongly suggests that the model is not correct and possibly that a

different film is growing on the Si surface which traces out a different  $\psi, \Delta$  trajectory.

In the effort to better determine the nature of the new film forming on the Si surface, in-situ contact angle measurements have proven useful(37). First it was observed that the contact angle,  $\theta$ , on  $\text{SiO}_2$  on Si was about  $8^\circ$  which indicates strong hydrophilic behavior of  $\text{SiO}_2$  as anticipated for a high energy solid in contact with an essentially aqueous media. When  $\theta$  is followed during HF in  $\text{H}_2\text{O}$  etching of  $\text{SiO}_2$ , an abrupt change from  $8^\circ$  to  $78^\circ$  occurs when the  $\text{SiO}_2$  is thought to be removed (near 2nm  $\text{SiO}_2$ ). The abrupt change from hydrophilic to hydrophobic behavior is a commonplace observation in HF treatment of a  $\text{SiO}_2$  covered Si surface(42). However, based on what we know about the surface energy of Si, namely it is high, the bare Si surface should be hydrophilic as is  $\text{SiO}_2$ , and thus no abrupt change in  $\theta$  is expected. We conclude that there is something else on the Si surface, something other than  $\text{SiO}_2$  or bare Si. In order to elucidate the nature of the hydrophobic Si surface resulting from HF exposure, the critical surface tension  $\gamma_c$  was measured. For this purpose, a plot of measured  $\cos\theta$  versus  $\gamma_{lv}$  is obtained on the Si surface in contact with a number of liquids with various  $\gamma_{lv}$  and all with HF. This was done using solutions of  $\text{H}_2\text{O}-\text{CH}_3\text{OH}$  all with 1% HF.  $\gamma_{lv}$  varied from 72 dynes/cm for pure  $\text{H}_2\text{O}$  to 23 dynes/cm for pure HF. Figure 11 shows the plot. First it is seen that the plot is not linear. This has been shown to be the case whenever H bonding between liquid and solid can occur (40)

which is expected for  $H_2O-CH_3OH$  solutions. More importantly is the extrapolated value of  $\gamma_c = 27$  dynes/cm for  $\cos\theta = 1$ . A comparison with literature values of  $\gamma_c$  leads to the conclusion that the new film on Si is either a hydrocarbon and/or fluorocarbon species. Since F is present and indeed crucial, and F-C bonds are polar enough to cause H bonding between Si and liquid, we conclude that a fluorocarbon is adsorbed on the Si surface.

It is interesting that this fluorocarbon film on Si renders the surface hydrophobic thereby likely precluding much foreign and potentially degrading impurities from attaching to an otherwise high energy Si surface. In addition, this treatment leads to clean MOS devices. The effect of a final HF treatment is essentially to yield the largest oxidation rate in comparison with other accepted cleaning solutions, e.g.,  $H_2O_2$ , HCl,  $NH_4OH$  (8). It is not yet known why this is the case and other effects of HF have not been determined, e.g. any long term effects of residual F after thermal oxidation.

#### Summary

The details of the mechanism for the reaction between Si and oxidant to form an  $SiO_2$  film is complex with many aspects: chemical, mechanical, electrical, morphological etc.. Many reviews on silicon oxidation have treated the problem in detail. The present paper focuses on two very recent results, namely mechanical intrinsic film stress implications and impurity

effects on the oxidation mechanism. For these new studies, novel techniques were used and are in themselves interesting means to study surface films. The results, while by no means have settled the major issues, have helped to gain further insight into the important problem of the mechanism for Si oxidation.

Acknowledgement

The author is indebted to G. Gould and E. Kobeda for access to their original data and for helpful discussions. This work was supported in part by the Office of Naval Research, ONR.

## References

1. E.A. Irene, Semiconductor International, April 1983, p. 99.
2. E.A. Irene, Semiconductor International, June 1985, p. 92.
3. B.E. Deal and A.S. Grove, J. Appl. Phys., 36, 3770 (1965).
4. W.A. Pliskin, IBM J. Res. Dev., 10, 198 (1966).
5. E.A. Irene and Y.J. van der Meulen, J. Electrochem. Soc., 123, 1380 (1976).
6. A.G. Revesz and R.J. Evans, J. Phys. Chem. Solids, 30, 551 (1969).
7. F.N. Schwettmann, K.L. Chiang and W.A. Brown, 153rd Electrochem. Soc. Meeting, Abs. #276, May 1978.
8. G. Gould and E.A. Irene, J. Electrochem. Soc., 134, 1031 (1987).
9. E.A. Irene, Phil. Mag. B, 55, 131 (1987).
10. E.A. Irene, CRC Reviews in Solid State and Materials Science, "Models for the Oxidation of Silicon," in press 1987.
11. R.J. Jaccodine and W.A. Schlegel, J. Appl. Phys., 37, 2429 (1966).
12. M.V. Whelan, A.H. Gormans and L.M. Goossens, Appl. Phys. Lett., 10, 262 (1967).
13. E.P. EerNisse, Appl. Phys. Lett., 30, 290 (1977); 35, 8 (1979).
14. E.A. Irene, E. Tierney and J. Angillelo, J. Electrochem. Soc. 129, 2594 (1982).
15. T.Y. Tan and U. Goesele, Appl. Phys. Lett., 39, 86 (1981); 40, 616 (1982).
16. W.A. Tiller, J. Electrochem. Soc., 128, 689 (1981).
17. E. Kobeda and E.A. Irene, J. Vac. Sci. Technol. B, 4, 720 (1986).
18. E. Kobeda and E.A. Irene, J. Vac. Sci. Technol. B, 5, 15 (1987).
19. G.G. Stoney, Proc. R. Soc., London Ser. A 82, 172 (1909).
20. E. Kobeda and E.A. Irene, J. Vac. Soc. B., to be published 1987.

21. G.A. Rozgonzi and D.C. Miller, *Thin Solid Films*, 31, 185 (1976).
22. A. Segmuller, J. Angillelo, S.J. La Placa, *J. Appl. Phys.*, 51, 6224 (1980).
23. A.G. Blachman, *Metal. Trans.*, 2, 699 (1971).
24. E.A. Irene, *J. Electronic Mat.*, 5, 287 (1976).
25. A.K. Sinha, H.J. Levinstein, and T.E. Smith, *J. Appl. Phys.*, 49, 2423 (1985).
26. J.K. Srivastava and E.A. Irene, *J. Electrochemical Soc.*, 132, 2815 (1985).
27. A. Fargeix, G. Ghibaudo and G. Kamarinos, *J. Appl. Phys.*, 54, 2878 (1983); 54, 7153 (1983); 56, 589 (1984).
28. G. Camera Roda, F. Santarelli and G.C. Sarti, *J. Electrochem. Soc.*, 132, 1909 (1985).
29. R.H. Doremus, *Thin Solid Films*, 122, 191 (1984).
30. E.A. Irene, H.Z. Massoud and E. Tierney, *J. Electrochem. Soc.*, 133, 1253 (1986).
31. C.K. Huang, R.J. Jaccodine and S.R. Butler, Abs. 34, *Electrochemical Society Meeting, Extend. Abstracts, Vol. 86-2, San Diego, CA, Oct. 19-24 (1986)*.
32. E.A. Lewis, E. Kobeda and E.A. Irene, "Proceedings of Fifth International Symposium on Silicon Materials Science and Processing," Ed. H.R. Huff, Boston, Mass., May 1986.
33. E.A. Lewis and E.A. Irene, *J. Electrochem. Soc.*, 134, 2332 (1987).
33. E.A. Irene, H.Z. Massoud and E. Tierney, *J. Electrochem. Soc.*, 133, 1253 (1986).
34. W. Kern, *Semiconductor International*, p. 94, April 1984.
35. B.F. Phillips, D.C. Burkman, W.R. Schmidt and C.A. Petersen, *J. Vac. Sci. Technol. A*, 1, 646 (1983).
36. R.C. Henderson, *J. Electrochemical Soc.*, 119, 772 (1972).
37. G. Gould and E.A. Irene, *J. Electrochem. Soc.*, submitted 1987.
38. R.M.A. Azzam and N.M. Bashara, "Ellipsometry and Polarized Light," North Holland Publishing Co., New York (1977).
39. Zisman, "Contact Angle: Wettability and Adhesion," *Advances in*

Chemistry Series Vol. 43, Ed. F.M. Fowkes, American Chem. Soc.,  
Washington, DC (1964), Chap. 1.

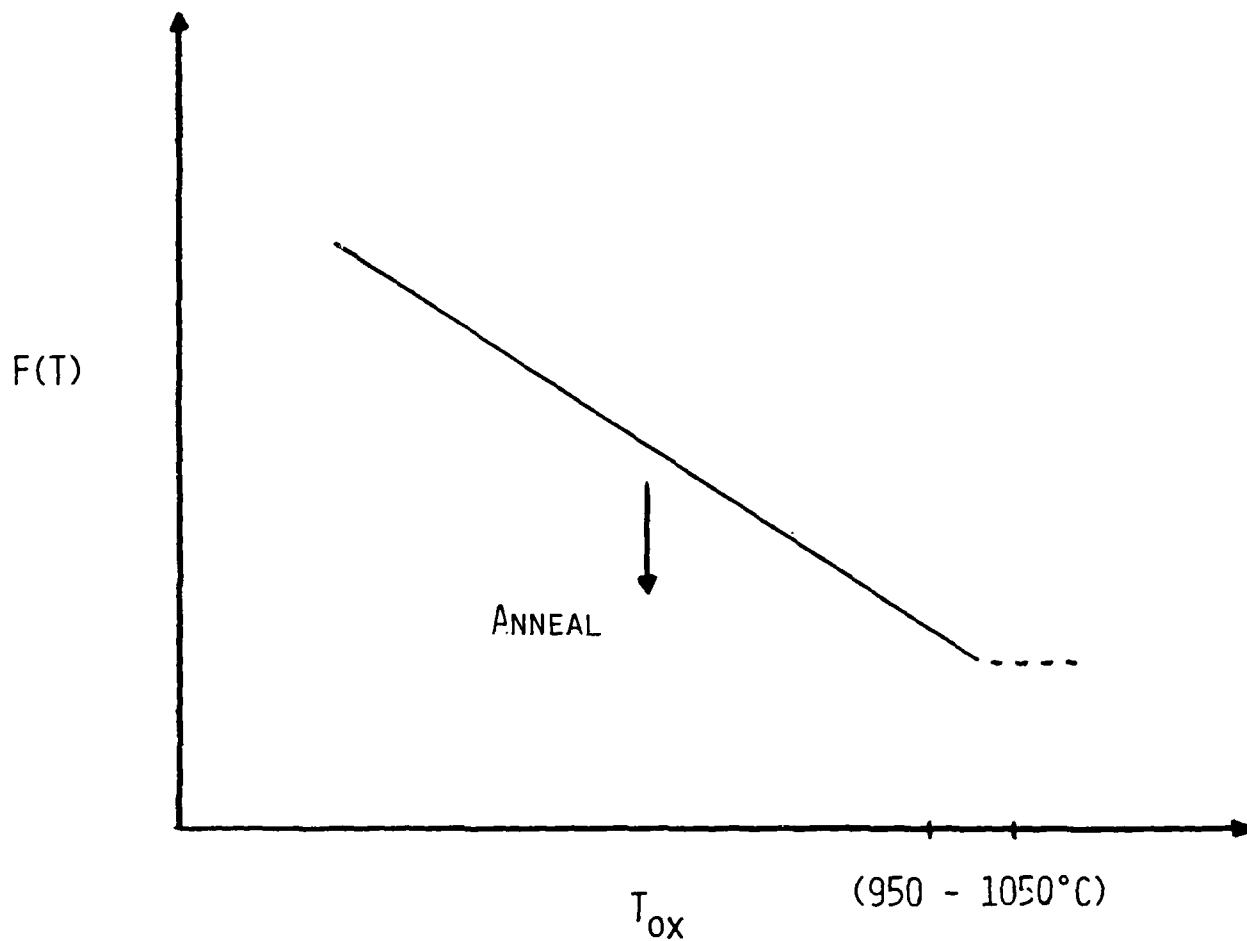
40. D. McLachlan Jr., and H.M. Cox, Rev. Sci. Instrum., 46, 80  
(1975).
41. E.A. Irene, Phil. Mag. B., 55, 131 (1987).
42. R. Williams and A.M. Goodman, App. Phys. Lett., 25, 531 (1974).

## List of Figures

- Figure 1. A schematic summary of  $F(T)$  versus oxidation temperature,  $T_o$ , where  $F(T)$  are the various oxidation temperature sensitive properties for  $\text{SiO}_2$  such as: refractive index, density, intrinsic stress, interface fixed charge, and interface trapped charge. (after ref. (41) and with permission of Phil. Mag.).
- Figure 2. Parallel laser beam apparatus for the measurement of wafer curvature. BS is a beamsplitter and MS is a flat mirror. (after ref. (17) and with permission of the American Vacuum Society).
- Figure 3. Total measured  $\text{SiO}_2$  film stress and calculated thermal expansion stress for various oxidation temperatures for  $\text{SiO}_2$  grown on Si in dry  $\text{O}_2$ . (after ref. (17) and with permission of the American Vacuum Society.)
- Figure 4. Intrinsic film stress versus oxidation temperatures for  $\text{SiO}_2$  film grown on Si in dry  $\text{O}_2$ . (after ref. (17) and with permission of the American Vacuum Society.)
- Figure 5. Pictorial representation of viscous flow in  $\text{SiO}_2$  as a result of the molar volume change for the reaction of  $\text{Si} + \text{O}_2 = \text{SiO}_2$  (after ref. (14) and with permission of the Electrochemical Society, Inc.)
- Figure 6. Intrinsic stress for a  $\text{SiO}_2$  film on Si versus oxidation temperature in dry  $\text{O}_2$  at one atm. for various Si orientations (after ref. (18) and with permission of the American Vacuum Society).
- Figure 7. Fused silica sample cell used for in-situ ellipsometric measurements. (after ref. (37)).
- Figure 8. Representation of the important surface tension vectors,  $\gamma_{ij}$ , for the equilibrium between solid, S, liquid, L, and vapor, V, and with  $\theta$  as the contact angle. (after ref. (37)).
- Figure 9.  $\text{SiO}_2$  film thickness versus etch time in HF- $\text{H}_2\text{O}$  solution from in-situ ellipsometry measurements (after ref. (37)).
- Figure 10.  $\Psi$ -vs- $\Delta$  trajectories for the etching of an 85nm  $\text{SiO}_2$  film in HF- $\text{H}_2\text{O}$  solution (after ref. (37)).
- Figure 11.  $\cos\theta$ -vs- $\gamma_{lv}$  plot of  $\text{SiO}_2$  on Si in various  $\text{CH}_3\text{OH}-\text{H}_2\text{O}-\text{HF}$  solutions.  $\gamma_c$  is shown at  $\cos\theta = 1$  to be 27 dynes/cm. (after ref. (37)).

SiO<sub>2</sub> FILM PROPERTIES, F(T), VERSUS OXIDATION

TEMPERATURE, T<sub>ox</sub>



F(T)	
INTRINSIC STRESS	$\sigma_i$
DENSITY	$\rho$
REFRACTIVE INDEX	$n$
FIXED OXIDE CHARGE	$Q_F$
INTERFACE TRAPPED CHARGE	$Q_{IT}$

Fig 1.

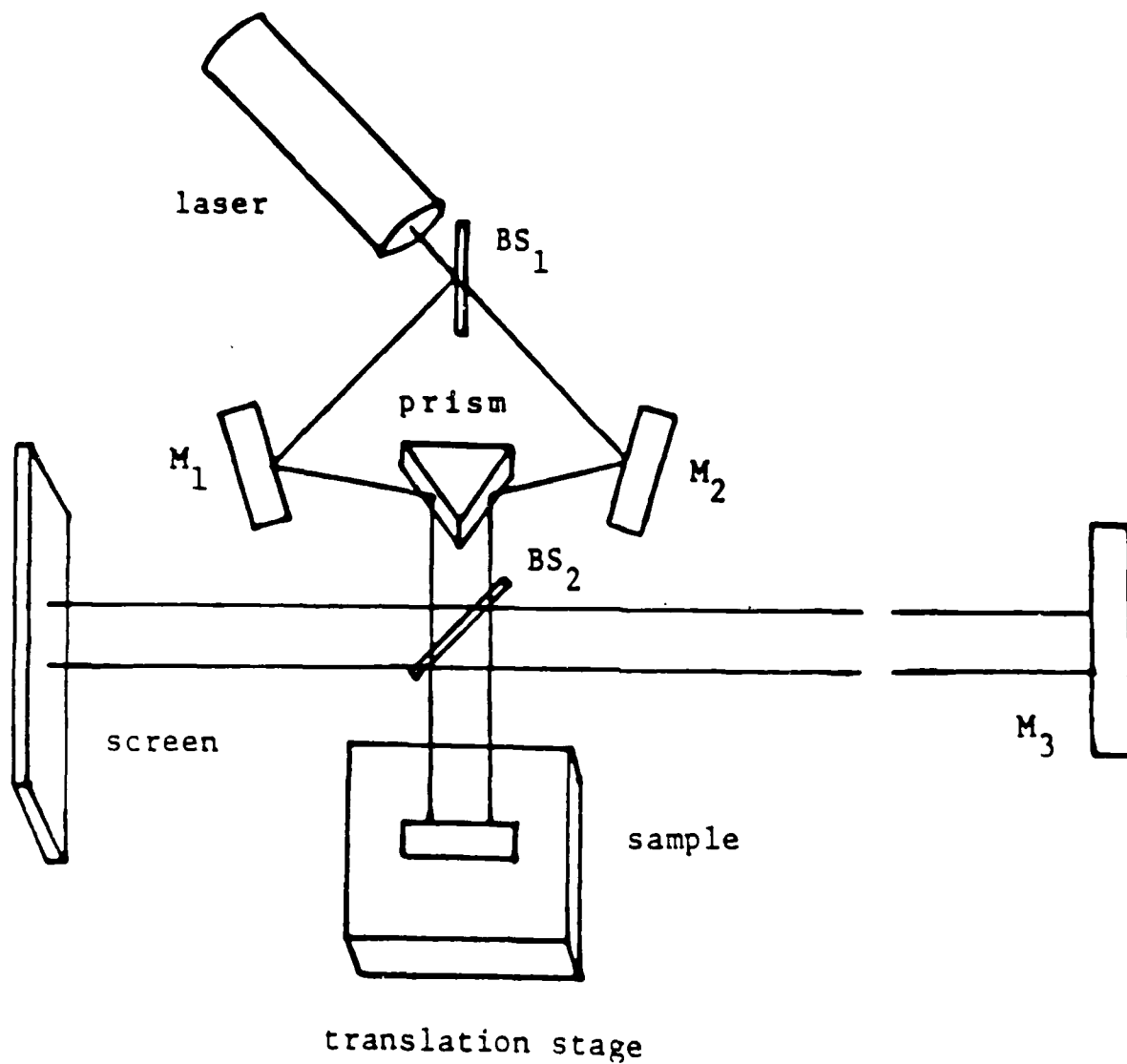


Fig 2

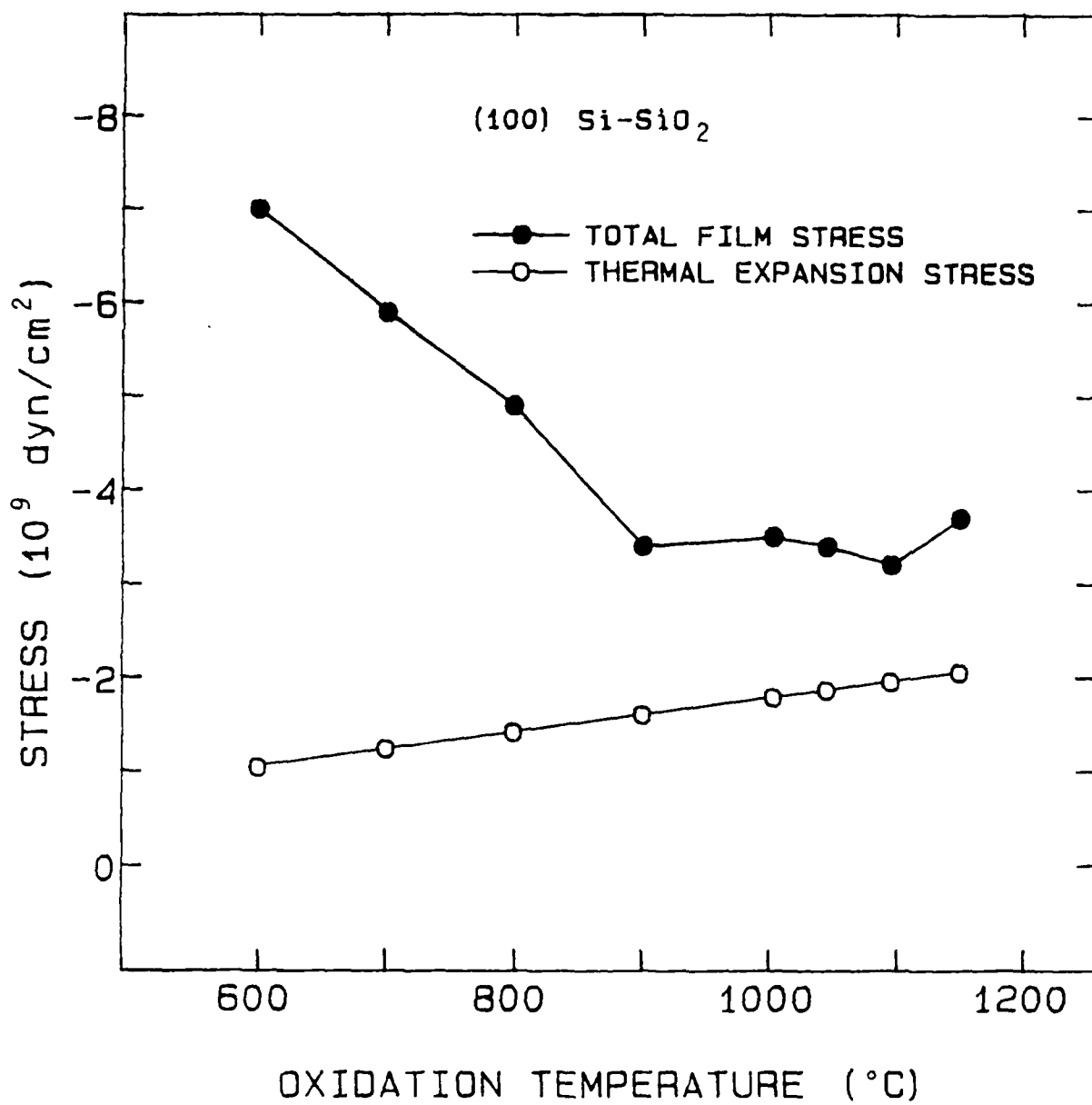


Fig 3

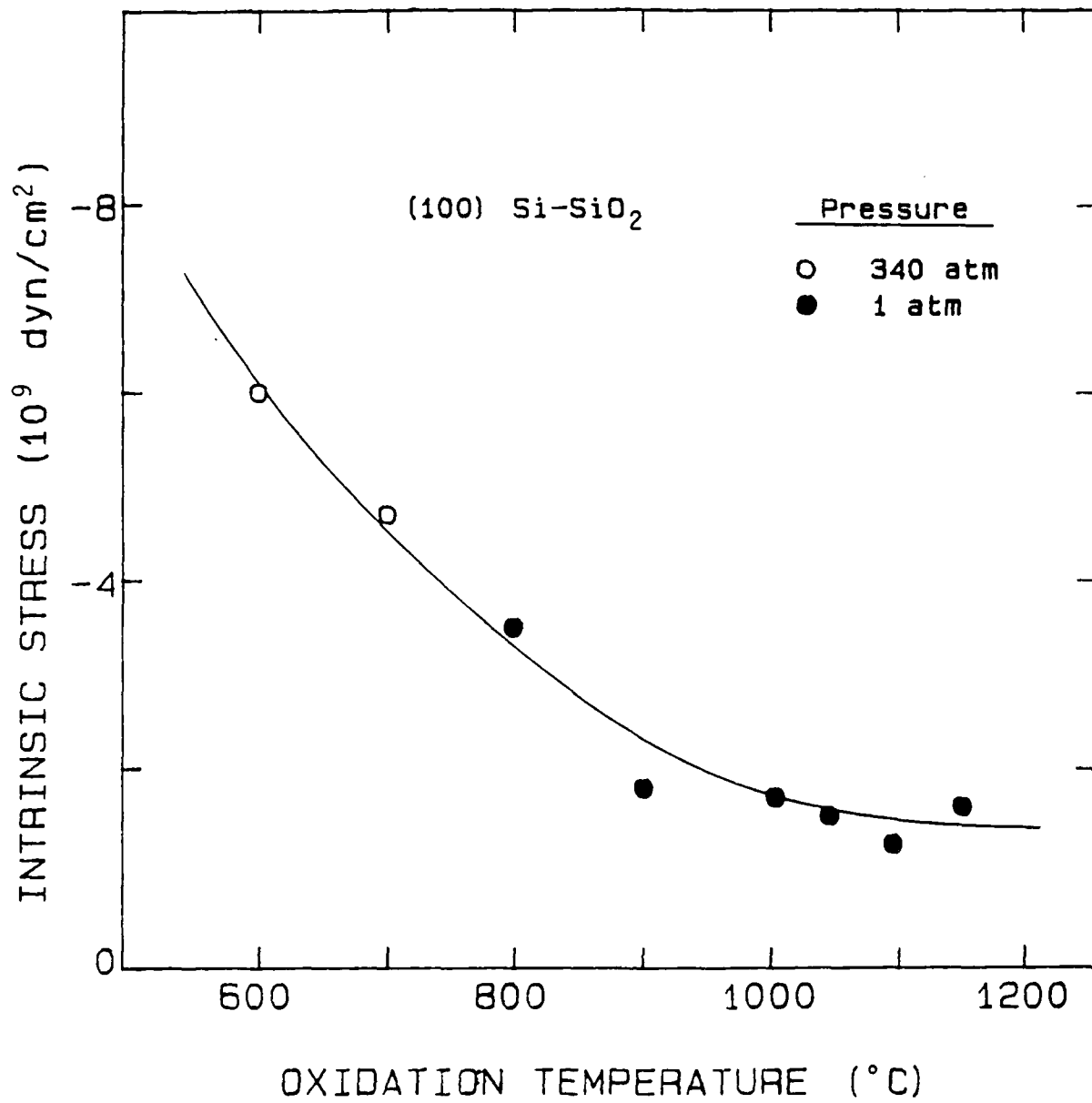
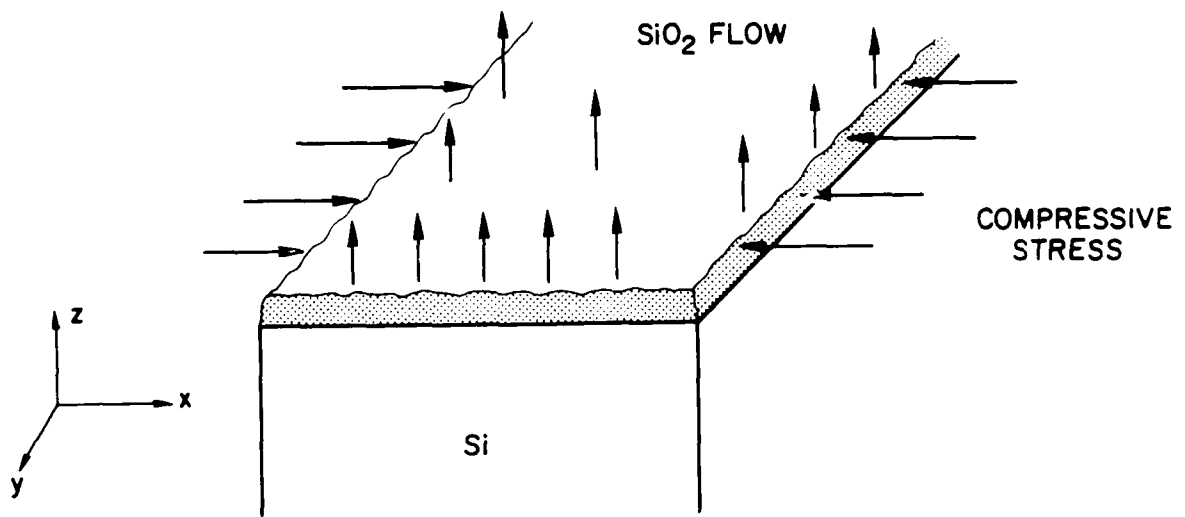


Fig 4



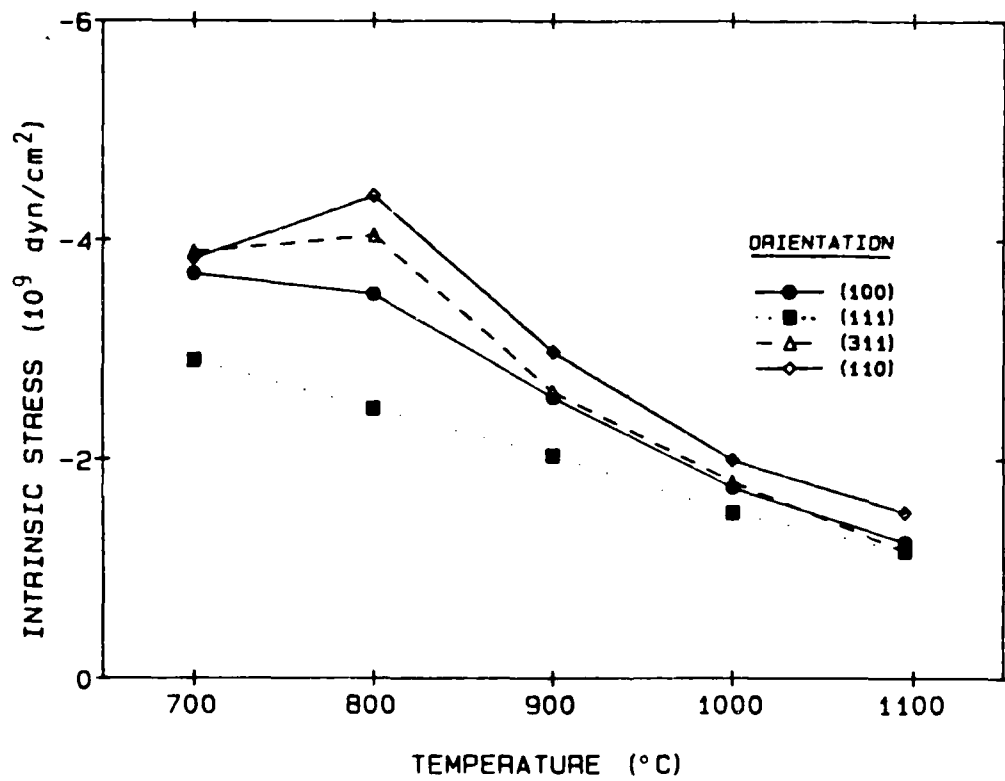


Fig. 6.

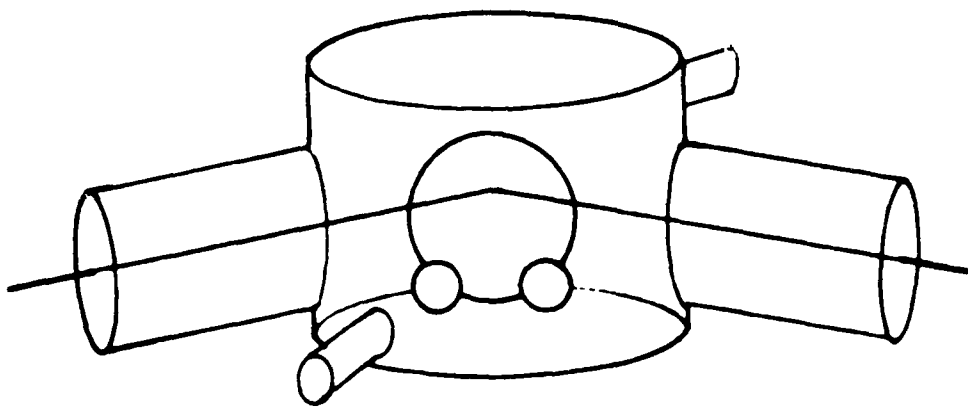


Fig. 17

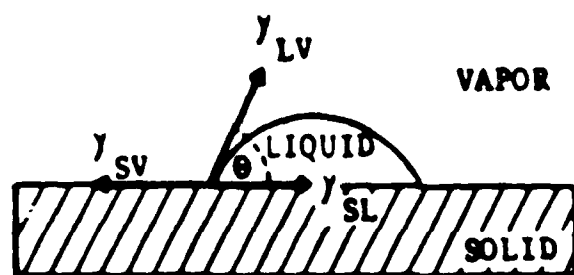
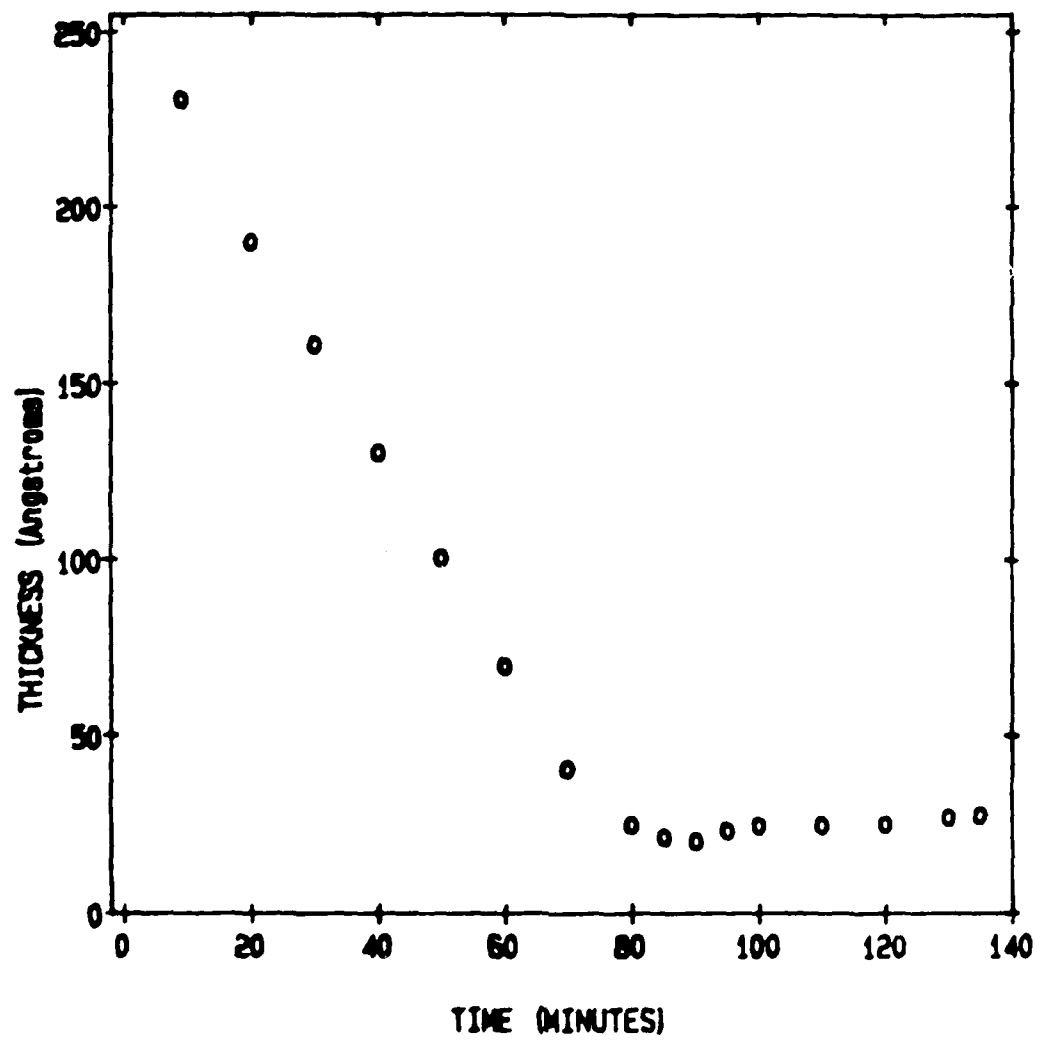
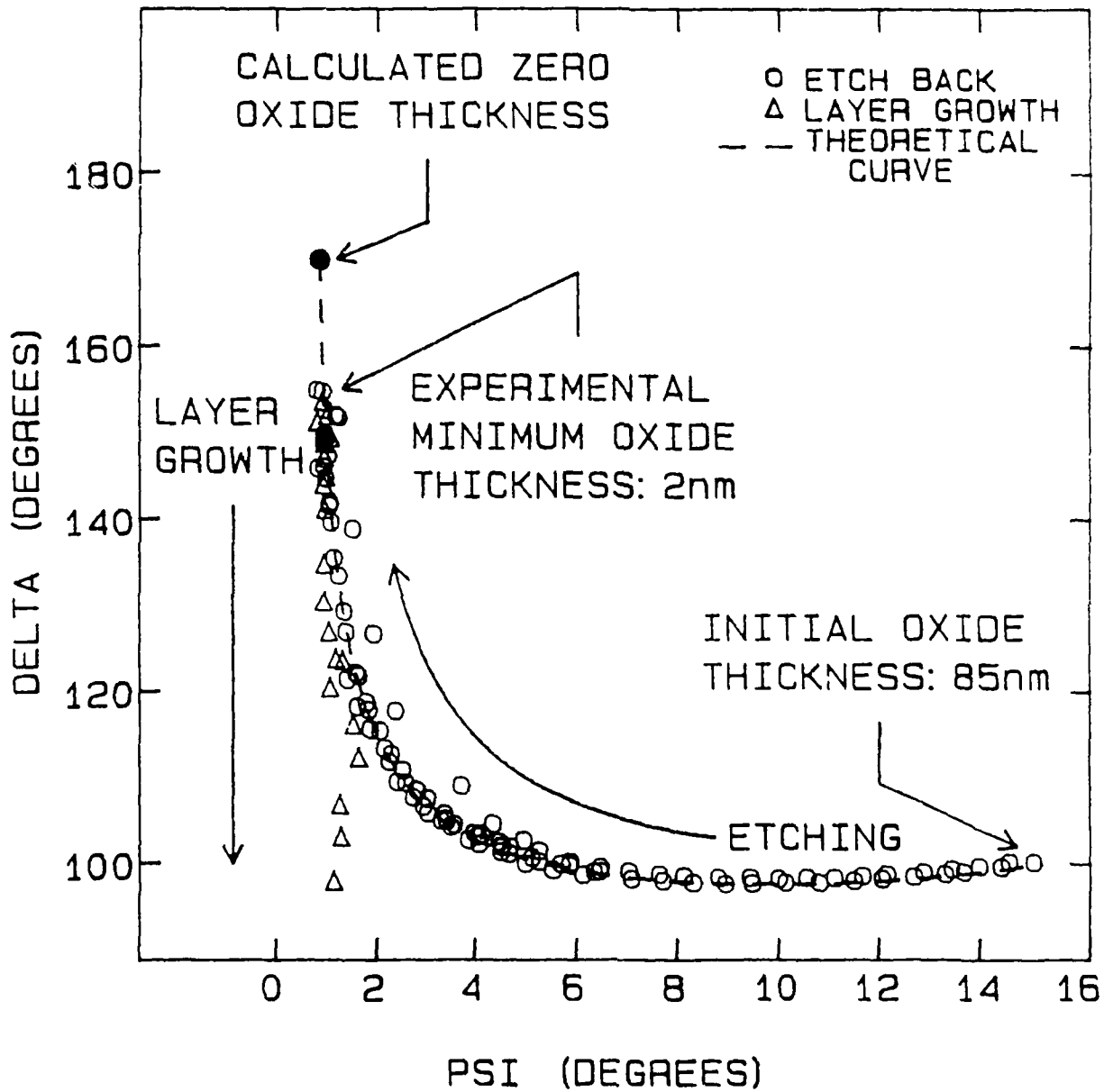


Fig 8



# PSI vs. DELTA FOR HF ETCH EXPERIMENTS



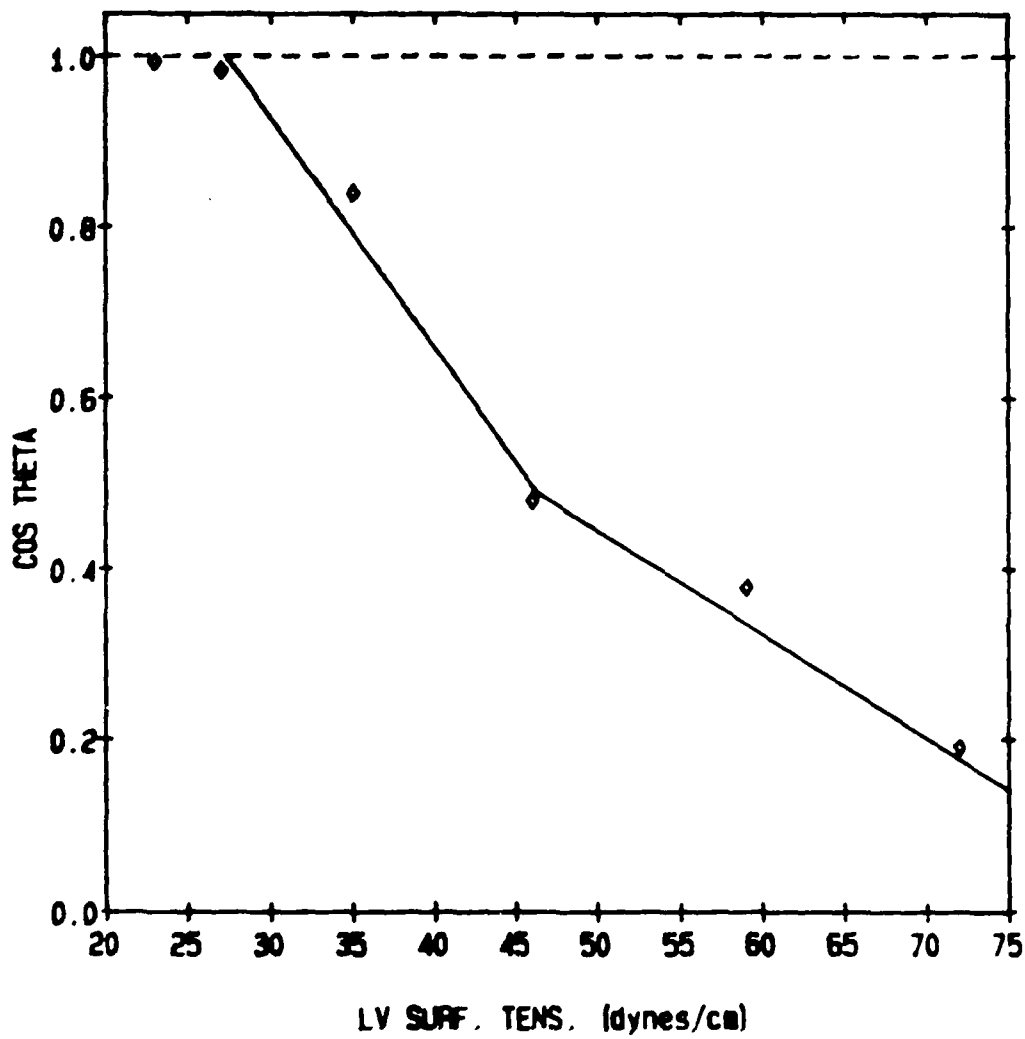


Fig 1

END

FILMED

MARCH, 19 88

DTIC